

## A bioactive titanium foam scaffold for bone repair

Erik D. Spoerke<sup>a</sup>, Naomi G. Murray<sup>a</sup>, Huanlong Li<sup>b</sup>, L. Catherine Brinson<sup>a,b</sup>,  
David C. Dunand<sup>a</sup>, Samuel I. Stupp<sup>a,c,d,\*</sup>

<sup>a</sup> Department of Materials Science and Engineering, Northwestern University, Evanston, IL 60208, USA

<sup>b</sup> Department of Mechanical Engineering, Northwestern University, Evanston, IL 60208, USA

<sup>c</sup> Department of Chemistry, Northwestern University, Evanston, IL 60208, USA

<sup>d</sup> Feinberg School of Medicine, Northwestern University, Chicago, IL 60611, USA

Received 10 January 2005; received in revised form 4 April 2005; accepted 6 April 2005

### Abstract

While titanium has been clinically successful as an orthopedic or dental implant material, performance problems still persist related to implant–bone interfacial strength and mechanical modulus mismatch between titanium and tissue. We describe here the preparation of a titanium foam as a better mechanical match to tissue with surfaces attractive to bone cells through deposition of an organically-modified apatite layer (organoapatite). In a rotating bioreactor, these organoapatite-coated foams are successfully colonized by preosteoblastic cells. Finite element analyses suggest that ingrown tissue in these systems may improve both implant performance and tissue formation through load-sharing and stress distribution. The novel metal–ceramic–polymer hybrid materials described here hold great promise for bone tissue engineering.

© 2005 Acta Materialia Inc. Published by Elsevier Ltd. All rights reserved.

**Keywords:** Porous titanium; Organoapatite; Hydroxyapatite; Bioreactor; Osteoblasts; Finite element model; Stress-shielding

### 1. Introduction

Titanium (Ti) and its alloys continue to be utilized extensively for skeletal repair and dental implants. Titanium's excellent strength-to-weight ratio, toughness, and most importantly, the biocompatibility and corrosion resistance of its naturally forming surface oxide have led to widespread clinical success [1–4]. There are, however, unresolved technical problems associated with using titanium as an implant material. The bioinert character of its protective surface oxide does not readily form a strong interface with surrounding tissue. Furthermore, the relatively high stiffness of titanium, as

compared to surrounding bone, can lead to problems of stress-shielding and subsequent implant loosening.

One approach to resolving the interface problem involves coating titanium surfaces with hydroxyapatite, the principal mineral in bones and teeth. Methods such as plasma spraying [5,6], sol–gel [7], electrophoretic deposition [8], and even solution phase apatite growth [9,10] have all been explored. Mechanical evaluation of extracted hydroxyapatite-coated implants has shown evidence of increased interfacial strength compared to implants with bare titanium surfaces [11–13]. Stupp et al. [14–16] previously developed materials known as organoapatites (OA) which incorporate 2–3% poly(L-lysine) into the mineral hydroxyapatite. The inclusion of these macromolecules into the mineral phase mimics some natural biogenic minerals containing small amounts of occluded proteins that regulate crystal formation and also toughen otherwise brittle matrices [17–19]. Previous *in vivo* work showed that organoapatite

\* Corresponding author. Address: Department of Materials Science and Engineering, Northwestern University, 2220 Campus Dr., Evanston, IL 60208, USA. Tel.: +1 847 491 3002; fax: +1 847 491 3010.

E-mail address: [s-stupp@northwestern.edu](mailto:s-stupp@northwestern.edu) (S.I. Stupp).

promotes not only bone apposition, but also interfacial resorption and bony replacement [16]. We have developed a method to grow OA on titanium-based implant surfaces, with the expectation that it may serve as an agent to encourage new bone growth at the implant interface before being resorbed and recycled [20]. The organoapatite coating is grown out of solution onto a double layer of oppositely charged poly(amino-acids) bound to titanium's natural oxide surface. This growth process offers a number of significant advantages over current coating procedures. The solution-phase nature of the growth allows for the coating of interior surfaces of porous structures, unlike directionally restricted methods such as plasma spraying. Furthermore, methods such as plasma spraying, sol-gel, and electrophoresis may produce highly crystalline coatings, which are difficult to resorb. The low density, nanocrystalline character of OA is expected to be more susceptible to natural remodeling processes, critical to maintaining the body's natural tissue. The deposition of organoapatite on titanium surfaces has been shown to enhance their colonization by bone cells [21].

A second approach to enhancing implant interfacial strength utilizes a porous implant surface, created by plasma spraying or surface sintering titanium powder or wires onto a solid implant surface [22–24]. Such systems rely on bone ingrowth into the shallow porous surface layer to stabilize the implant. An improvement on this concept is to use a titanium foam presenting porosity not only at the implant surface but throughout the entire structure. This scheme may allow for a greater degree of bony infiltration, while also reducing the stiffness of the foam as compared to that of solid titanium, thereby addressing the stress shielding problem. Stress shielding refers to the condition whereby fully dense titanium, which is significantly stiffer than bone, shields surrounding tissue from stresses, resulting in interfacial resorption and implant loosening. As reviewed recently [25], three-dimensionally porous titanium can be produced by various sintering methods, including partial sintering of powders [26,27] or wires [28], or by sintering of powders around a temporary space-holding phase [29,30], but the resulting structure is relatively weak, due to the small necks connecting the individual powder particles. An alternative foaming method for Ti alloys was developed by Kearns et al. [31,32]. Micron-size bubbles of pressurized inert argon gas are entrapped within a titanium matrix during consolidation of titanium powders by hot isostatic pressing (HIPing). Upon subsequent exposure to elevated temperatures and ambient pressure, these bubbles expand by creep of the titanium matrix, resulting in formation of a titanium foam with up to approximately 50% porosity. As compared to foams produced by powder sintering, these foams exhibit higher strength because of the more rounded pore shape and full density of struts [33].

In this work, we report on the synthesis of hybrid titanium foams in which porous surfaces have been modified by osteoconductive organoapatite layers. We study the *in vitro* colonization of the foams by bone cells and also predict the hybrid material's mechanical interactions with ingrowing tissue through finite element (FE) modeling.

## 2. Methods and materials

The foaming process was previously described by Davis et al. [34]. Spherical CP-Ti powders (–100 mesh size) with median size of  $\sim 130\ \mu\text{m}$  were packed to approximately 70% density in a steel can. The can was evacuated, back-filled with 3.3 atm Ar, sealed, and then subjected to HIPing at 890 °C and 100 MPa for 125 min. Cubic specimens with approximately 6 mm edges were cut from the consolidated billet, encapsulated in evacuated quartz capsules and introduced in a preheated furnace at 960 °C and foamed for a total of 24 h. Total specimen porosity was determined by Archimedes density measurements on samples sealed with a thin layer of vacuum grease in distilled water. Density measurements were also performed using helium pycnometry on unsealed specimens, allowing for measurement of closed porosity.

Foamed titanium was cut with a diamond-coated abrasive saw into samples 4 mm  $\times$  4 mm  $\times$  1 mm, and 1 mm diameter holes were drilled through the samples for skewering in a bioreactor. These substrates were cleaned ultrasonically for 15 min each in reagent-grade dichloromethane, reagent-grade acetone, and de-ionized water. Pores clogged by metal smearing during cutting were opened by etching in a 0.25% HF, 2.5% HNO<sub>3</sub> solution for 45 min. Samples were then re-passivated in 40 vol.% HNO<sub>3</sub> solution for 30 min, and rinsed with de-ionized water. The processes for sample pretreatment and growth of organoapatite were adapted from previous work [20,21] for application with the titanium foam. Foam samples were suspended in a Teflon sample holder and pretreated for 22 h in poly(L-lysine) (pLys) at pH 7.4, followed by 20 h in poly(L-glutamic acid) (pGlu) at pH 7.4. Organoapatite precipitation was conducted by combining 500 mL each of 15 mM calcium hydroxide and 9 mM phosphoric acid solutions with 400 mL of 1 mM poly(L-lysine) at 37 °C and pH 7.4. Collected precipitate was partially dissolved by addition of HCl. Pretreated samples were then introduced to the partially dissolved organoapatite and the OA was reprecipitated by the dropwise addition of 3 M NaOH restoring pH to 7.4. After several hours, samples were rinsed with de-ionized water and dried under vacuum. Non-adherent precipitate was rinsed and vacuum desiccated for later analysis.

Surface analysis of the OA-coated foam substrates was performed on gold/palladium-coated samples by

field-emission scanning electron microscopy (SEM) (Hitachi model S-4500) at an accelerating voltage of 20 kV. Transmission electron microscopy (TEM) (Hitachi, model 8100) was used to analyze organoapatite morphology and crystal structure as established by electron diffraction of OA directly grown on a Ti grid and also on precipitated OA. These samples were examined in a Hitachi 8100 transmission electron microscope at an accelerating voltage of 200 keV.

Non-adherent OA precipitate was further characterized by powder X-ray diffraction with a Rigaku D-Max X-ray instrument at 40 kV and 20 mA using CuK $\alpha$  radiation to confirm the formation of organoapatite by comparison to JCPDS data for hydroxyapatite (JCPDS #09-0432). Organoapatite powder was also mixed with potassium bromide and pressed into pellets for Fourier transform infrared spectroscopy (FTIR) using a Bio-Rad FTS-40 FTIR spectrophotometer. Bulk samples were furthermore submitted for elemental analysis of calcium and phosphorus content (University of Illinois Microanalytical Laboratory, Urbana, Champaign).

MC3T3-E1 osteogenic murine calvaria cells were used in these experiments. Cells were maintained in a T-75 flask at 37 °C and 8% CO<sub>2</sub>, using  $\alpha$ -modified Eagle's medium (MEM- $\alpha$ ), supplemented with 10% fetal bovine serum (FBS), 100 units/mL of penicillin and streptomycin, 3 mM  $\beta$ -glycerol phosphate, and 50  $\mu$ g/mL ascorbic acid. Cells were removed from the flask surface by treatment with 0.25% trypsin, 1 mM ethylenediaminetetraacetic acid and loaded into a 110 mL STLV rotating bioreactor culture vessel (Synthecon, Houston, TX). Foam samples, sterilized in an autoclave at 121 °C for 50 min, were skewered onto a steel wire sample holder through the hole drilled in the samples. Samples were separated by poly(tetrafluoroethylene) spacers and different sample types were arranged on separate skewers. This sample holder was inserted into the bioreactor culture vessel filled with 10<sup>7</sup> cells in culture medium described above. This vessel was then rotated at 15 r.p.m. in an incubator at 37 °C and 5% CO<sub>2</sub>, exchanging half of the culture medium approximately every 3 days.

To insure reproducibility all measurements were taken three times each for duplicate samples and the entire experiment was repeated three times. Specimens were harvested after 1, 7, 14, and 28 days and fixed for 1 h with 2.5% glutaraldehyde in 0.1 M sodium cacodylate buffer (pH 7.4). Specimens were washed sodium cacodylate buffer before post-fixing with 1% aqueous osmium tetroxide for 1 h. Water-rinsed samples were then dehydrated into ethanol, critical point dried by ethanol-CO<sub>2</sub> exchange, and coated with 3 nm gold-palladium for examination by SEM at an accelerating voltage of 10 kV.

Additional samples were harvested, fixed, and dehydrated into ethanol before embedding in LR White.

Slices of the embedded material were then cut with a diamond saw, thinned by polishing and stained in haematoxylin for analysis by optical microscopy.

Alkaline phosphatase activity was determined as a function of the alkaline phosphatase-catalyzed production of *p*-nitrophenol from *p*-nitrophenol phosphate, measured by monitoring light absorbance at 410 nm (Sigma Kit 245) on a Cary 500 UV-VIS spectrometer. Cell proliferation was measured on ALP samples after ALP measurements were taken. Samples were placed in papain protease solution for cell digestion over the course of 16 h at 60 °C, as adapted from the protocol described by Allen et al. [35]. Liberated DNA in solution was combined with Hoechst 33258 and quantified by fluorescence on an ISS PC1 fluorescent spectrophotometer. The number of cells from each mesh sample was estimated from this measured quantity of DNA, assuming that one cell contains 7.7 pg of DNA [36].

Osteocalcin was qualitatively identified in these experiments using a method similar to the process described by Attawia et al. [37]. Cells were trypsinized from foam substrates and plated onto tissue-culture polystyrene well-plates. After 8 h cells were fixed at 4 °C for 1 min with a solution of 70% ethanol, 25% distilled water, and 5% acetic acid. Fixed cells were rinsed in phosphate buffered saline (PBS) and incubated for 30 min in 1% bovine serum albumin (BSA). Double-antibody immunohistochemistry was then performed using goat anti-mouse osteocalcin as the primary antibody (Biomedical Technologies, Inc., Stoughton, MA) and a fluorescently tagged donkey anti-goat secondary antibody (Molecular Probes, Eugene, OR).

Finite element models were created to predict the potential behavior of these foam implants in vivo, especially the localized mechanical properties that cannot be directly observed from experiments. Based on approximations from the experimental data collected in the experiment, a commercial FE software package (ABAQUS Standard 6.3-1) was used to create two-dimensional meshes, representative of 25% porous foam microstructures with 25 round pores, whose size and position were randomly perturbed from an average value and a regular 5  $\times$  5 array, respectively. Pores were selectively filled with inclusions with the mechanical properties of bone to simulate the effects of bone ingrowth within the pores of the foam structure. Foam constructs were sandwiched between model layers of bone, representing bony tissue adjacent to an implant. Four mesh structures were utilized in the FE simulations: foam with empty pores (E-P), foam where outer pores only were filled with bone (OF-P) simulating partial bone ingrowth, foam where all pores were filled with bone (AF-P), and solid titanium (S). The material properties used for the simulations are displayed in Table 1. The modulus, yield stress, and strain hardening behavior for titanium was determined from a stress-strain curve

Table 1  
Mechanical properties used for finite element simulations

	E (GPa)	$\nu$	$\sigma_{\text{yield}}$ (MPa)
Titanium	110	0.33	275
Bone	20	0.30	120

for CP-40 titanium [38], and moderate values for dense cortical bone were obtained from the literature [39–41]. Due to lack of reliable data for plasticity hardening curves for bone, a perfect elastic–plastic approximation was used. Standard linear quadrilateral elements were defined for the entire geometry and plane strain conditions were applied during simulation. Simulation constraints were set such that only the bottom boundary and the bottom left corner were fixed. All nodes along the right and left boundaries (bone–air interface) were traction free, and all material interfaces assumed perfect bonding. The boundary conditions were not periodic to better represent the conditions of a real structural implant in situ. Simulations were conducted under a compressive traction boundary condition of 7 MPa distributed uniformly along the top surface of the model, whose magnitude was determined according to femoral load approximations for a 90–100 kg human walking or climbing stairs [42,43]. Further simulations were conducted to determine the sample moduli and the onset of local plastic deformation by incremental displacement (0–0.1% strain) of the top of the sample under plane strain conditions.

### 3. Results

The isothermal foaming of titanium proceeded as previously described, producing a foam of approximately 25% porosity, with only 3% open to the surface [34]. This specimen porosity was achieved after about 1 h at 960 °C, as the titanium matrix crept under the stresses produced by the pressurized gas in the pores. As the pore volume increased, the corresponding reduc-

tion of gas pressure rapidly reduced the stresses responsible for pore expansion, resulting in reduction and eventual cessation of foaming. During the remaining 23 h of the thermal treatment, pore coalescence, visible in Fig. 1b, occurred together with the opening of some pores to the specimen surface, releasing the pressurized gas. While only approximately one-eighth of the total porosity was open to the specimen surface after the 24 h thermal treatment, this effect also contributed to the cessation of foaming.

As shown in Fig. 1a, initial pores in the HIPed billets retained the general shape of the gap between powders in the original preforms, and were thus non-spherical. The initial average pore size was on the order of 10–25  $\mu\text{m}$  and the initial porosity was measured by the Archimedes procedure to be about 0.55%. Fig. 1b shows the pore structure in CP-Ti after foaming for 5.25 h at 960 °C. The pores were rounded and had a diameter of up to 200  $\mu\text{m}$  (many of the smaller pores result from the metallographic plane intersecting far from the equatorial plane of the roughly spherical pore) with a total porosity of approximately 22%.

The compressive behavior of the foam was ductile, with a yield stress of about 200 MPa. Young's moduli for all specimens were found from the stress–strain curves to be 40 GPa with a large error of  $\pm 20$  GPa. Ultrasonic evaluation of the elastic constants for a foam processed at 960 °C with 22% porosity gave a Young's modulus of 60 GPa.

Characterization by X-ray diffraction of organoapatite (OA), shown in Fig. 2a, revealed a hydroxyapatite crystal structure, shown by elemental analysis to be slightly calcium deficient ( $\text{Ca/P} = 1.55\text{--}1.60$ ). The FTIR spectra in Fig. 2b confirmed this to be an apatitic structure with characteristic bands at 567, 605, 964, 1037, and 1100  $\text{cm}^{-1}$ . Poly(L-lysine) present and associated with the apatitic phase was also indicated by an amide I band ( $\text{C=O}$  stretch) at 1650  $\text{cm}^{-1}$  [44,45]. Elemental analysis of carbon and nitrogen further confirmed the presence of approximately 2–3% poly(L-lysine) in the organoapatite mineral. The transmission electron micrograph of

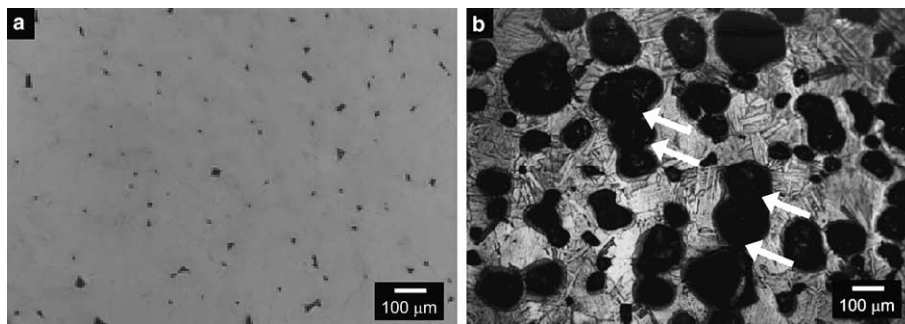


Fig. 1. (a) Optical micrograph of as-HIPed titanium microstructure showing pressurized Ar pore before expansion. (b) Optical micrograph of titanium foamed at 960 °C for 5.25 h with 22% porosity. Arrows indicate pore coalescence.

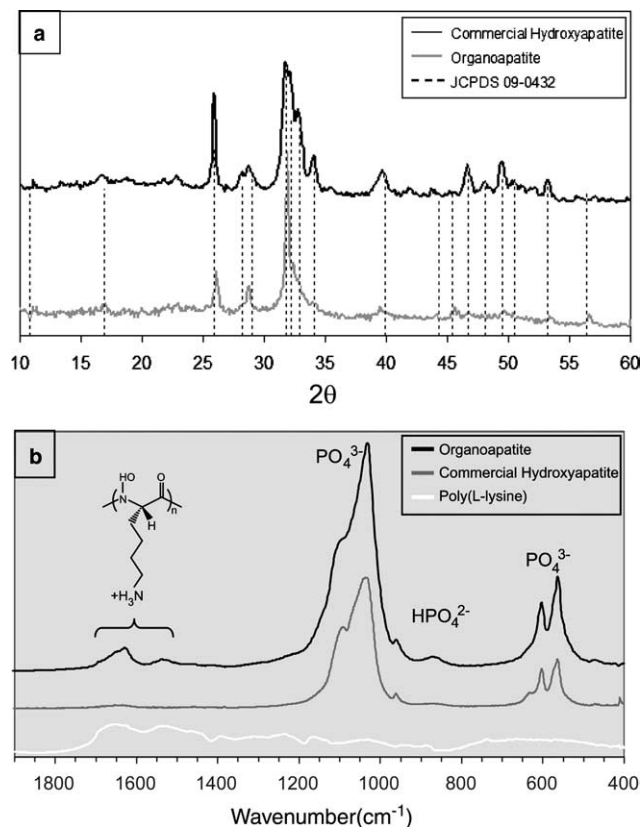


Fig. 2. (a) Powder X-ray diffraction spectra for non-adherent OA precipitate, and commercial HA. Dotted lines represent hydroxyapatite peaks as described by JCPDS file 09-0432. (b) Fourier transform infrared spectra comparing OA, commercial HA, and poly(L-lysine).

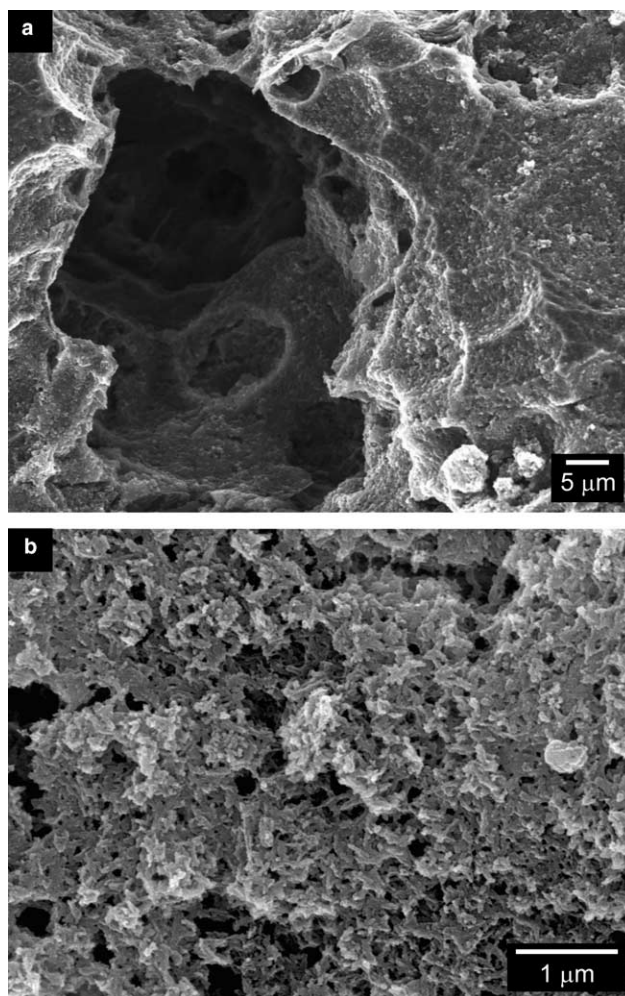


Fig. 4. Organoapatite grown on titanium foam. (a) Coralline OA texture observed on the foam surface and inside pores. (b) High magnification image of the coralline texture of OA on the foam surface.

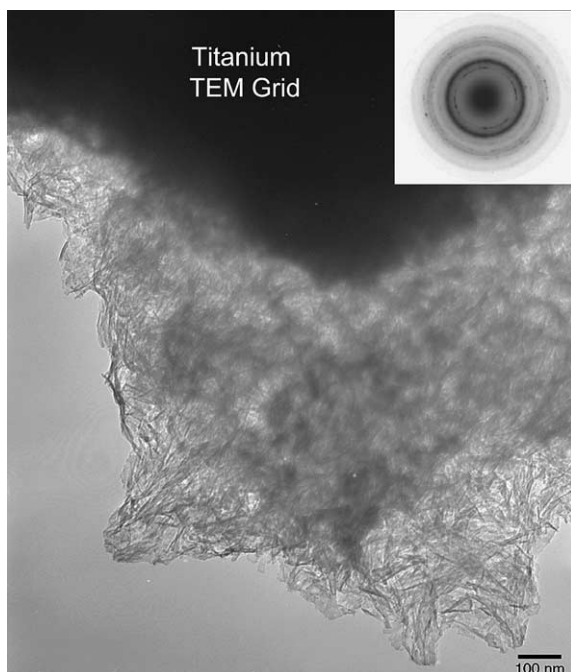


Fig. 3. A transmission electron micrograph of OA crystals grown off a titanium TEM grid. Inset diffraction pattern (upper right) of OA nanocrystals shows polycrystalline rings and arcs which match diffraction spacings for hydroxyapatite.

OA grown on a Ti TEM grid is shown in Fig. 3. OA crystals appeared as elongated plates consistently on the order of 30–40 nm wide, 50–100 nm long, and 10–15 nm thick, dimensions similar to those of naturally forming biological apatite [40]. The coralline structures seen in the micrographs in Fig. 4 are aggregates of these plate-like apatite nanocrystals, covering 70–80% of the foam surfaces, including pore interiors. The high magnification image in Fig. 4b shows these finely textured organoapatite aggregates grown on the titanium surfaces. The structures observed were similar to those previously observed on Ti surfaces [20,21].

Cells were found to effectively seed the foam substrates in the dynamic environment of the rotating bioreactor. Cellular colonization of organoapatite-coated foam was tracked visually by SEM, and more quantitatively by cellular proliferation. Fig. 5 illustrates this colonization through 14 days of culture. In Fig. 5a, cells are seen attached to OA-covered textures of a pore edge on

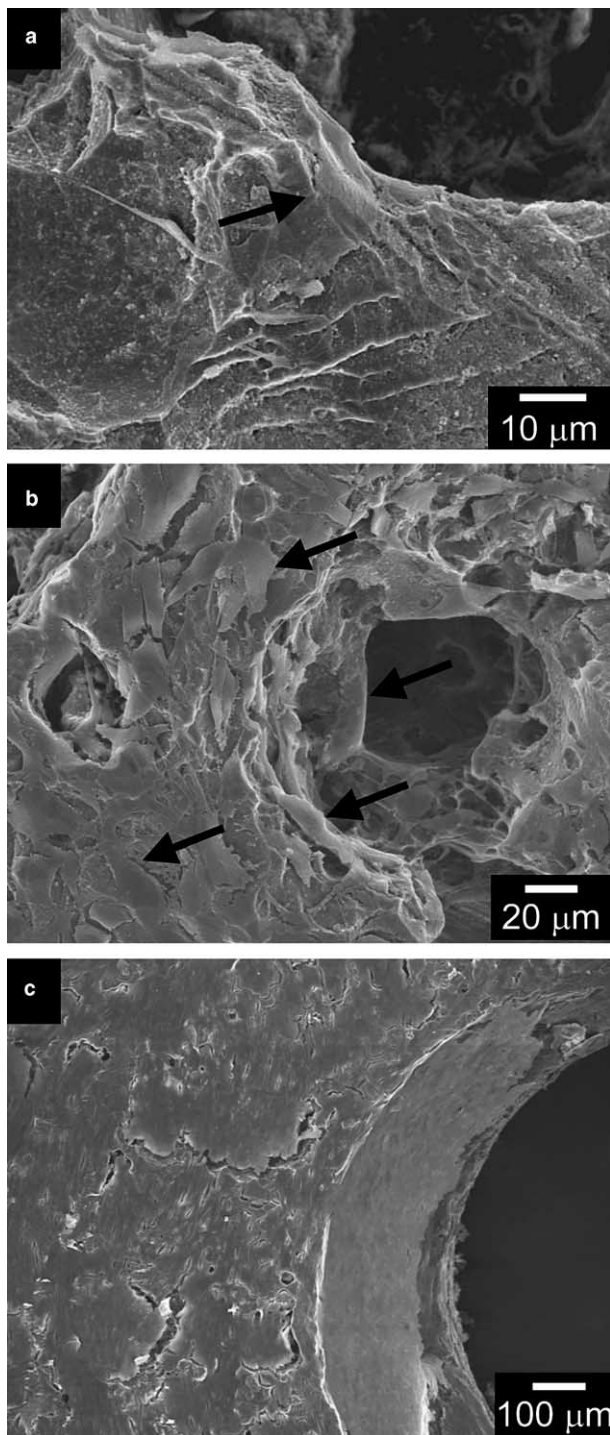


Fig. 5. SEM micrographs of cell colonization on OA–Ti foam: (a) a cell is visible (arrow) attaching to the edge of an OA-coated pore after 1 day of culture; (b) after 7 days, cells (arrows) have proliferated, covering foam surfaces and extending within foam pores; (c) by 14 days, cells have completely colonized the OA–Ti foam surface with a layer of cells.

the foam surface after 1 day of culture. Fig. 5b shows that by 7 days the cells had proliferated on the OA-coated foam surfaces and had begun to grow into foam pores. Cell numbers measured at these early time points,

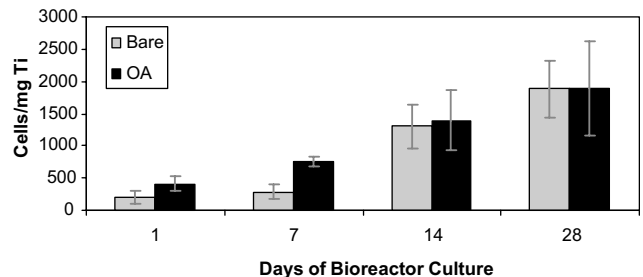


Fig. 6. Proliferation of preosteoblastic cells on OA-coated and bare titanium foam. Total DNA measured was normalized by foam sample mass. Error bars are  $\pm 1$  standard deviation.

shown in Fig. 6, indicate more cells present on OA-coated samples than on bare controls. By 14 days, confluent cell layers had completely overtaken the porous foam surface, seen in Fig. 5c, and the proliferation data in Fig. 6 show that there was no longer a significant difference in the number of cells growing on OA-coated samples versus bare controls. SEM examination of pores with openings approximately 75–200  $\mu\text{m}$  wide, however, reveals that at later stages of growth, cells were more consistently found in OA-coated pores than in bare pores, a difference illustrated in Fig. 7. The scanning electron micrograph in Fig. 7a shows cells climbing down the walls of a relatively large OA-coated pore, while the optical micrograph in Fig. 7b illustrates cells filling a smaller pore. In contrast the images in Figs. 7c and d depict cells bridging over bare titanium pores. Regardless of the presence of OA, however, cells tended to bridge virtually all pores smaller than 75  $\mu\text{m}$ , and to grow into pores larger than 200  $\mu\text{m}$ . In all cases, cellular infiltration of the foam was limited to exterior and surface-connected pores. This observed model corresponds well with the partially-filled OF-P model simulated in FE analysis.

Alkaline phosphatase measured from these cell-coated foams shows that by 14 days of cellular colonization, these preosteoblastic cells had begun to upregulate their alkaline phosphatase expression, indicating osteoblastic differentiation (see Fig. 8a). This effect increased dramatically by 28 days. The OA coating did not appear to either inhibit, or enhance the rate or intensity of expressed alkaline phosphatase. Osteocalcin was also expressed in cells from OA-coated foams after 28 days of culture. Fig. 8b shows a fluorescent image of cells, grown on an OA-foam, expressing osteocalcin. As with the ALP, there was no apparent influence of the OA coating on the rate or intensity of osteocalcin expression.

The FE modeling showed that porous models were completely elastic up to 0.11% uniaxial external strain (0.14% for the fully bone-filled model), whereas the solid titanium model was completely elastic through 0.25% strain. The elastic modulus calculated from the FE analysis of the foam constructs (E-P) was 57.4 GPa, a value

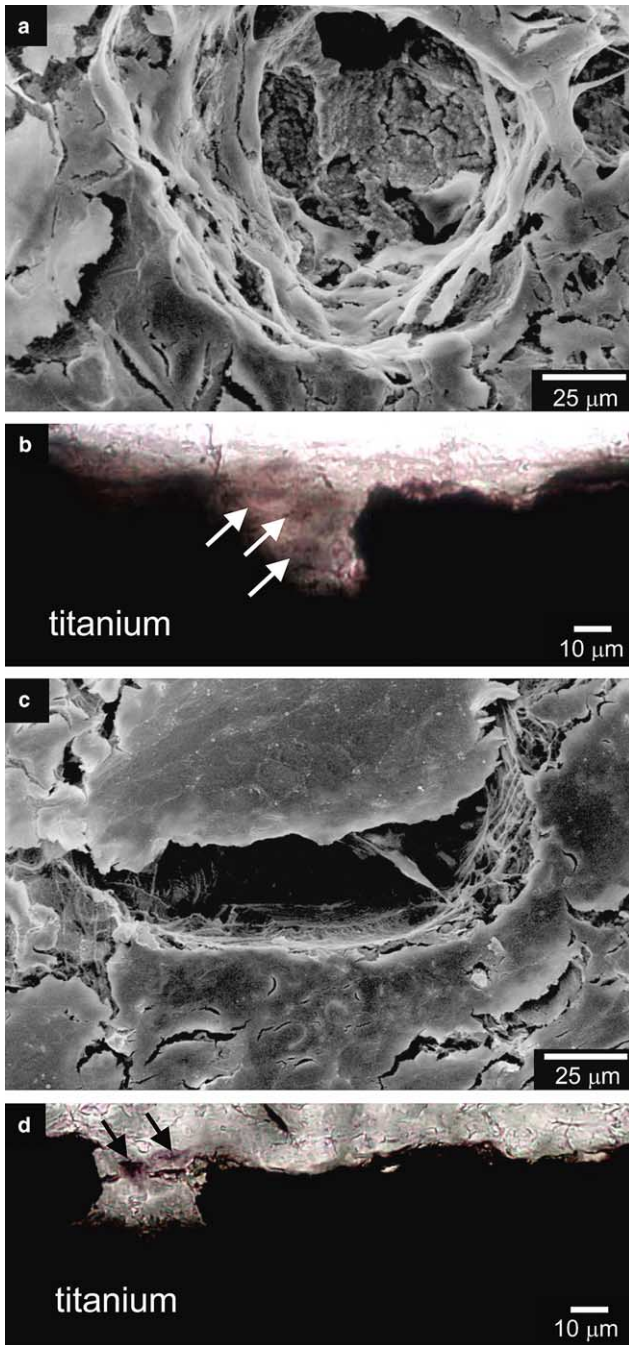


Fig. 7. (a) SEM micrograph and (b) cross-sectional optical micrograph of cells growing into OA-coated pores; (c) SEM micrograph and (d) cross-sectional optical micrograph of cells bridging over a bare titanium pore. Cells in cross-sectional micrographs, purple oval structures indicated by arrows, were stained with haematoxylin.

in good agreement with the ultrasonically determined modulus of the foam reported above (60 GPa), and was substantially lower than the modulus of solid Ti (110 GPa). The foam modulus increased to 64.9 GPa for the model with outer pores only filled (OF-P) and 72.9 GPa in the model with all pores filled (AF-P).

The relative decrease in modulus for these foamed structures, compared with solid Ti, correlated directly

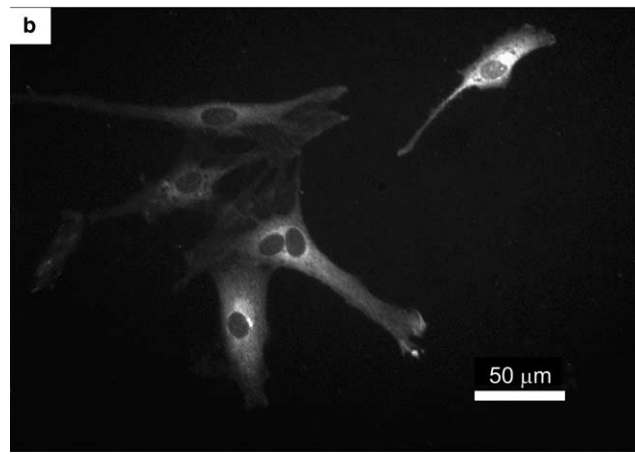
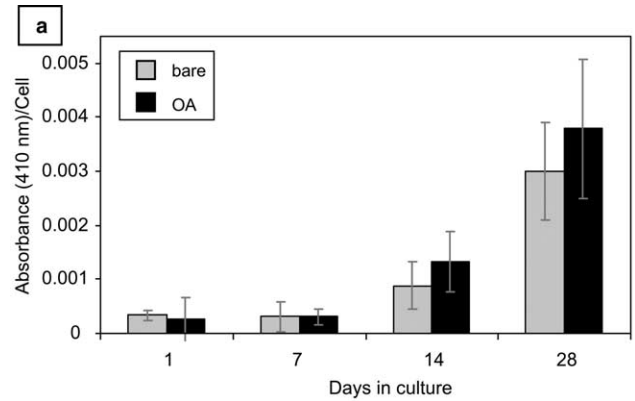


Fig. 8. (a) Alkaline phosphatase (ALP) expression from cells grown on OA-coated and bare titanium foam. ALP was normalized by the number of cells on each sample. (b) Double-antibody-stained fluorescent image of osteocalcin-expressing preosteoblast from an OA-foam sample after 28 days of culture. Similar expression was observed for bare samples (not shown).

with the degree of stress the titanium structures shared with surrounding bone. This effect is visually evident in the FE maps showing spatial distribution of the von Mises equivalent stress, shown in Fig. 9, for samples subjected to 7 MPa uniaxial pressure. The lighter blue colors seen in the surrounding bone for the porous models indicate larger stresses compared to the bone in the solid model, evidence that the host bone shared a larger fraction of the overall load for a porous implant. The image of the particularly stiff solid titanium material in Fig. 9 displays a greater predominance of the low-stress (dark blue) regions in the surrounding bone when compared to the porous foam models. Within these porous models, regions of relatively higher stress in the surrounding bone (light blue) shrank as the pores filled with bone, increasing the titanium–bone composite modulus. In addition, the ratio of the average stress found in surrounding bone to the average applied stress, plotted in Fig. 9, provides a quantitative measure of this stress-sharing effect. The porous sample (E-P) demonstrated a significant increase in the amount of stress shared with

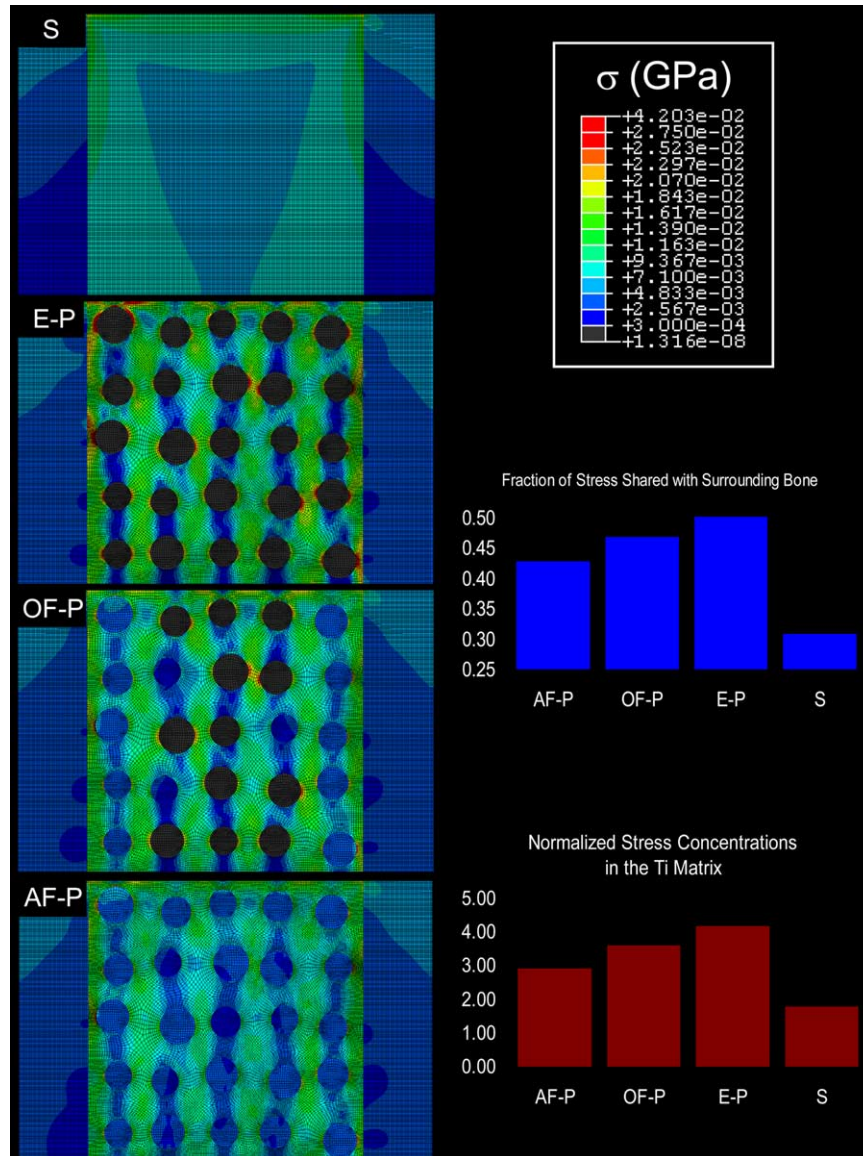


Fig. 9. Maps of von Mises equivalent stress in FE models of solid titanium (S), empty pore foam (E-P), foam with outer pores filled with bone (OF-P), and foam with all pores filled with bone (AF-P). Each substrate was encased within bone and images are shown for an applied uniaxial compressive stress of 7 MPa. Plots show the ratio of the average stress found in surrounding bone to the average applied stress (above) and the ratio of maximum stress in the Ti matrix of each foam structure to the average stress seen in the solid implant case.

surrounding bone (ratio = 0.53), as compared to the stress-shielded condition found with the solid Ti (ratio = 0.31). This stress-sharing effect persisted in the two bone-filling models, OF-P (ratio = 0.46) and AF-P (0.43), but as the modulus of the foam construct rose with increased bone content, the degree of load sharing with surrounding bone decreased.

Filling the pores with bone had an additional influence on the stress distribution in these models, as it served to reduce stress concentrations in the titanium matrix, an effect also visible in Fig. 9. The red and yellow regions in these images indicate regions of high stress. Furthermore, to quantitatively compare stress concentrations between models, the ratio of maximum

stress in the Ti matrix of each composite structure to the average applied stress was calculated and plotted in Fig. 9. In the uniform, solid titanium structure, this ratio was relatively low (ratio = 1.8), indicating that there were no significant local stress concentrations, an effect visually emphasized by the absence of red or yellow stress indicators in the solid Ti graphic. In the E-P foam, however, some regions of the titanium phase surrounding open pores were subjected to more than three times the average stress (ratio = 4.2), and the images in Fig. 9 show clear evidence of a significant stress concentrations around the discontinuous geometry of the foam pores. Filling the pores with bone, however, clearly reduced the magnitude of these stresses. In the OF-P mod-

el, only pores filled with bone showed substantial reduction of stress (ratio = 3.6). The greatest reduction of these stress concentrations was observed when all the pores were filled with bone, evidenced by the disappearance of the red and yellow high stress indicators in Fig. 9 as well as by the decrease in the measured stress ratio (2.9).

#### 4. Discussion

We have described here the synthesis of an organoapatite-coated titanium foam, probed its *in vitro* interactions with bone cells cultured in a rotating bioreactor, and modeled the behavior of these foam structures as bone implants using finite element analysis. In the high-temperature foaming process used [32,34,46], the pressurized argon bubbles, internally trapped during HIPing, created stresses sufficient to expand within the creeping surrounding titanium matrix. The resulting material was a three-dimensionally porous titanium foam with excellent matrix integrity and strength. This foamed material, coated with the osteoconductive organoapatite, showed potential as an orthopedic implant system based on its interactions with bone cells, particularly at very early stages. Furthermore, the finite element results indicate that in addition to the OA-coated foams serving as suitable porous substrates for cell colonization, the foams influence on stress redistribution may prove valuable in stimulating osteogenesis and preventing implant failure by increasing the percentage of load shared by host bone.

Dynamically seeded on organoapatite-coated foams in the rotating bioreactor, preosteoblastic cells spread and began osteoblastic differentiation on the coating both on foam exterior surfaces as well as inside surface-connected foam pores. As with any *in vitro* scaffold seeding experiment, the true complexity of the *in vivo* process can not be exactly reproduced. It is possible that artificial events such as cell-scaffold collisions may have an influence on seeding behavior and warrant further study. On the other hand, compared with two-dimensional static seeding, the three-dimensional, dynamic nature of the seeding and colonization in the rotating bioreactor may better approximate the complex, efficient exchange of nutrients, waste, and cell signals prevalent in *in vivo* processes [47]. Empirically, this study shows that use of the rotating bioreactor is a viable and successful approach to culturing bone cells on titanium foam substrates.

In a previous study, it was shown that organoapatite had an influence on early seeding events of titanium mesh, leading to enhanced colonization by preosteoblasts [21]. Similar results were obtained here even though a very different, bioreactor-based seeding process was used. Organoapatite's unique combination of

calcium phosphate chemistry, nanocrystalline texture, and poly(L-lysine) content likely played key roles in promoting early cell attachment to the foams [48–52]. Naturally, cell attachment is a key step in creating a strong interface between an implant and native tissue. Establishing early bone cell attachment is clinically important in promoting more rapid healing and creating a more direct bone-implant interface at a time when early bone tissue growth may compete with fibrous tissue formation.

Most importantly though, the OA coating encouraged cell growth into foam pores connected to the samples surface, an effect consistent with the ability of organoapatite surfaces to promote bone cell colonization [21]. This effect may have resulted from improved cellular attachment inside the pores during seeding in the bioreactor. Alternatively, the cells seeded on the foam's exterior surface may have proliferated and migrated more readily into unseeded pores coated with OA. Such behavior is a consistent and valuable extension of previously observed preosteoblastic migratory colonization of unseeded, OA-coated Ti mesh. This enhanced colonization of the foam's surface-connected pores is expected to be important first because of the improved interfacial strength of a mechanical bond formed between ingrown tissue and the porous foam surface. Secondly, the FE analyses revealed that bony matrix infiltrated into the foam pores may substantially reduce local stress concentrations and delay the onset of plastic deformation, which in turn, should reduce the risk of implant failure due to local pore wall fracture by overload or fatigue. While the most significant reduction of stress concentration in the FE analyses occurred when all the pores of the foam were filled with bone, there was also significant stress reduction in the partially-filled OF-P model. Modeled after the experimental results described above where cells and matrix were grown into the foam's exterior surface pores, this partially-filled OF-P most accurately represents the cultured osteoblast-foam construct obtained in the bioreactor. This OF-P model does suggest then, that the cellular colonization of the OA-coated foam's exterior pores may prove valuable in reducing implant failure from local stress concentrations in the foam.

While the titanium foam remained quite strong ( $\sigma_y = 200$  MPa) with respect to bone ( $\sigma_y \sim 120$  MPa), the foam's three-dimensionally porous structure presented a significant decrease in macroscopic stiffness (60 GPa), compared to fully dense titanium (110 GPa). Though these experiments were conducted with foams of approximately 25% porosity, optimization of the foaming parameters can lead to porosity values as high as 45% [32,34,46,53–55]. By comparison, Ti powder sintering methods have been shown to produce foams in excess of 80% or 90% porosity [30,56,57]. These higher porosity foams would display further decreased stiffness

and potentially greater tissue ingrowth, but at the cost of strength, which would almost certainly decrease implant lifetime due to severe stress concentrations and fatigue damage. The present FE analysis suggests that the decrease in modulus seen with these strong and relatively dense 25% porous foams may be sufficient to reduce problems with stress shielding by promoting better macroscopic load sharing between an implant and the surrounding tissue. There are a number of reports suggesting that low magnitude mechanical stimulation might be beneficial to the osteogenic activity of bone cells [58–60]. Once again projecting the OF-P model on the experimental results from the bioreactor, the relatively low stiffness of the partially-infiltrated foam may facilitate the mechanical stimulation and load sharing not only with the surrounding bone, but also with the cells colonizing the surface-connected pores. Clearly, the loading model used for this FE analysis is simplified significantly with respect to the complex loading schemes in bone under physiological conditions. Our results, however, suggest that the reduced foam stiffness and the increased stress carried by the bone could positively influence osteogenesis at porous implant–tissue interfaces.

## 5. Conclusions

In vitro experiments in a rotating bioreactor demonstrated early colonization of organoapatite-coated titanium foams by preosteoblasts. Finite element simulations predict bony infiltration in the foam would not only create a stronger implant interface, but may also preserve the titanium implant lifetime through reduction of stress-concentration in the titanium matrix. The simulations also showed that utilization of a porous foam may serve to substantially reduce stress shielding problems, as compared to fully dense titanium.

## Acknowledgements

We would like to gratefully acknowledge funding support from the National Science Foundation (DMR0108342) and the Department of Energy (DEFG02-00ER45810). We would also like to acknowledge Professor Lonnie Shea in the Northwestern University Department of Chemical Engineering for donation of the MC3T3-E1 cell line.

## Supplementary data

Supplementary data associated with this article can be found, in the online version at [doi:10.1016/j.actbio.2005.04.005](https://doi.org/10.1016/j.actbio.2005.04.005).

## References

- [1] Laing PG. Tissue reaction in rabbit muscle exposed to metallic implants. *J Biomed Mater Res* 1967;1:135–49.
- [2] Albrektsson T et al. The interface zone of inorganic implants in vivo: titanium implants in bone. *Annals Biomed Eng* 1983;11:1–27.
- [3] Hayashi K, Uenoyama K, Matsuguchi N, Sugioka Y. Quantitative analysis of in vivo tissue responses to titanium-oxide and hydroxyapatite-coated titanium alloy. *J Biomed Mater Res* 1991;25:515–23.
- [4] Urban R, Jacobs J, Sumner D, Peters C, Voss F, Galante J. The bone–implant interface of femoral stems with non-circumferential porous coating—a study of specimens retrieved at autopsy. *J Bone Jt Surg—Am Vol A* 1996;78(7):1068–81.
- [5] de Groot K, Geesink R, Klein CPAT, Serekin P. Plasma-sprayed coatings of hydroxylapatite. *J Biomed Mater Res* 1987;21:1375–81.
- [6] Filiaggi MJ, Coombs NA, Pilliar RM. Characterization of the interface in the plasma-sprayed HA coating/Ti-6Al-4V implant system. *J Biomed Mater Res* 1991;25(10):1211–29.
- [7] Chai C, Ben-Nissan B. Bioactive nanocrystalline sol–gel hydroxyapatite coatings. *J Mater Sci—Mater Med* 1999;10(8):465–9.
- [8] Wei M, Ruys AJ, Swain MV, Kim SH, Milthorpe BK, Sorrell CC. Interfacial bond strength of electrophoretically deposited hydroxyapatite coatings on metals. *J Mater Sci—Mater Med* 1999;10(7):401–9.
- [9] Kokubo T, Miyaji F, Kim HM, Nakamura T. Spontaneous formation of bonelike apatite layer on chemically treated titanium metals. *J Am Ceram Soc* 1996;79(4):1127–9.
- [10] Wen H, de Wijn J, Cui F, de Groot K. Preparation of calcium phosphate coatings on titanium implant materials by simple chemistry. *J Biomed Mater Res* 1998;41(2):227–36.
- [11] Wang BC, Lee TM, Chang E, Yang CY. The shear strength and failure mode of plasma-sprayed hydroxyapatite coating to bone: the effect of coating thickness. *J Biomed Mater Res* 1993;27:1315–27.
- [12] Oonishi H et al. The effect of hydroxyapatite coating on bone growth into porous titanium alloy implants. *J Bone Jt Surg B* 1989;71:213–6.
- [13] Cook SD, Thomas KA, Dalton JE, Volkman TK, Whitecloud TSI. Hydroxylapatite coating of porous implants improves bone ingrowth and interface attachment strength. *J Biomed Mater Res* 1992;26:989–1001.
- [14] Stupp SI, Ciegler GW. Organoapatites: materials for artificial bone. I. Synthesis and microstructure. *J Biomed Mater Res* 1992;26:169–83.
- [15] Stupp SI, Mejicano GC, Hanson JA. Organoapatites: materials for artificial bone. II. Hardening reactions and properties. *J Biomed Mater Res* 1993;27:289–99.
- [16] Stupp SI, Hanson JA, Eurell JA, Ciegler GW, Johnson A. Organoapatites: materials for artificial bone. III. Biological testing. *J Biomed Mater Res* 1993;27:301–11.
- [17] Stupp SI, Braun PV. Molecular manipulation of microstructures—biomaterials, ceramics, and semiconductors. *Science* 1997;277:1242–8.
- [18] Albeck S, Addadi L, Weiner S. Regulation of calcite crystal morphology by intracrystalline acidic proteins and glycoproteins. *Connect Tissue Res* 1996;35(1–4):419–24.
- [19] Belcher AM, Wu XH, Christensen RJ, Hansma PK, Stucky GD, Morse DE. Control of crystal phase switching and orientation by soluble mollusc-shell proteins. *Nature* 1996;381(6577):56–8.
- [20] Hwang JJ, Jaeger K, Hancock J, Stupp SI. Organoapatite growth on an orthopedic alloy surface. *J Biomed Mater Res* 1999;47(4):504–15.

- [21] Spoerke E, Stupp SI. Colonization of organoapatite-titanium mesh by pre-osteoblastic cells. *J Biomed Mater Res* 2003;67(3):960–9.
- [22] Pilliar RM. Porous-surfaced metallic implants for orthopaedic applications. *J Biomed Mater Res—App Biomater* 1987;21(A1):1–33.
- [23] Simske S, Ayers R, Bateman T. Porous materials for bone engineering. *Mater Sci Forum* 1997;250:151–82.
- [24] Sumner D, Turner T, Urban R, Galante J. Remodeling and ingrowth of bone at 2 years in a canine cementless total hip arthroplasty model. *J Bone Jt Surg Am Vol A* 1992;74:239–50.
- [25] Dunand DC. Processing of titanium foams. *Adv Eng Mater* 2004;6(6):369–76.
- [26] Asaoka K, Kuwayama N, Okuno O, Miura I. Mechanical properties and biomechanical compatibility of porous titanium for dental implants. *J Biomed Mater Res* 1985;19(6):699–713.
- [27] Oh IH, Segawa H, Nomura N, Hanada S. Microstructures and mechanical properties of porosity-graded pure titanium compacts. *Mater Trans* 2003;44(4):657–60.
- [28] Murray GAW, Semple JC. Transfer of tensile loads from a prosthesis to bone using porous titanium. *J Bone Jt Surg—Br Vol* 1981;63(1):138–41.
- [29] Bram M, Stiller C, Buchkremer HP, Stover D, Baur H. High-porosity titanium, stainless steel, and superalloy parts. *Adv Eng Mater* 2000;2(4):196–9.
- [30] Wen C, Mabuchi M, Yamada Y, Shimojima K, Chino Y, Asahina T. Processing of biocompatible porous Ti and Mg. *Scripta Mater* 2001;45:1147–53.
- [31] Kearns M, Blenkinsop P, Barber A, Farthing T. *Met Mater* 1987;3(2):85.
- [32] Kearns MW, Blenkinsop PA, Barber AC, Farthing TW. Manufacture of a novel porous metal. *Int J Powder Metall* 1988;24(1):59–64.
- [33] Murray NGD, Dunand DC. Microstructure evolution during solid-state foaming of titanium. *Compos Sci Technol* 2003;63(16):2311–6.
- [34] Davis N, Teisen J, Schuh C, Dunand D. Solid-state foaming of titanium by superplastic expansion of argon-filled pores. *J Mater Res* 2001;16(5):1508–19.
- [35] Allen R, Eisenberg S, Gray M. Quantitative measurement of the biological response of cartilage to mechanical deformation. In: Morgan J, Yarmush M, editors. *Tissue engineering methods and protocols*. Totowa, NJ: Humana P; 1999. p. 536.
- [36] Kim Y-J, Sah R, Doong J-Y, Grodzinsky A. Fluorometric assay of DNA in cartilage explants using Hoechst 33258. *Anal Biochem* 1988;174:168–76.
- [37] Attawia M, Herbert K, Uhrich K, Langer R, Laurencin C. Proliferation, morphology, and protein expression by osteoblasts cultured on poly(anhydride-co-imides). *J Biomed Mater Res* 1999;48(3):322–7.
- [38] Boyer H. *Atlas of stress–strain curves*. Materials Park, OH: ASM International; 2002.
- [39] Katz J. Application of materials in medicine and dentistry: orthopedic applications. In: Ratner BD, Hoffman AS, Schoen FJ, Lemons JE, editors. *Biomaterials science: an introduction to materials in medicine*. San Diego, CA: Academic Press; 1996. p. 341–2.
- [40] Weiner S, Wagner H. The material bone: structure-mechanical function relations. *Annu Rev Mater Sci* 1998;28:271–98.
- [41] Reed K, Brown T. Elastic, yield and ultimate properties of emu cortical bone. *Iowa Orthop J* 2001;21:53–8.
- [42] Taylor S, Walker P. Forces and moments telemetered from two distal femoral replacements during various activities. *J Biomech* 2001;34:839–48.
- [43] Heller M et al. Musculo-skeletal loading conditions at the hip during walking and stair climbing. *J Biomech* 2001;34:883–93.
- [44] Lambert J, Shurvell H, Lightner D, Cooks R. *Group frequencies: infrared and Raman*. Introduction to organic spectroscopy. New York: Macmillan; 1987, p. 169–82.
- [45] Socrates G. *Infrared and Raman characteristic group frequencies*. 3rd ed. Chichester: John Wiley and Sons; 2001.
- [46] Murray NGD, Schuh CA, Dunand DC. Solid-state foaming of titanium by hydrogen-induced internal-stress superplasticity. *Scripta Mater* 2003;49(9):879–83.
- [47] Yu X, Botchway EA, Levine EM, Pollack SR, Laurencin C. Bioreactor-based bone tissue engineering: the influence of dynamic flow on osteoblast phenotypic expression and matrix mineralization. *Proc Natl Acad Sci* 2004;101(31):11203–8.
- [48] Kay S, Thapa A, Haberstroh K, Webster T. Nanostructured polymer/nanophase ceramic composites enhance osteoblast and chondrocyte adhesion. *Tissue Eng* 2002;8(5):753–61.
- [49] Catledge S et al. Nanostructured ceramics for biomedical implants. *J Nanosci Nanotech* 2002;2(3–4):293–312.
- [50] Gutwein L, Webster T. Osteoblast and chondrocyte proliferation in the presence of alumina and titania nanoparticles. *J Nanoparticle Res* 2002;4(3):231–8.
- [51] Jacobson B, Branton D. Plasma membrane: rapid isolation and exposure of the cytoplasmic surface by use of positively charged beads. *Science* 1977;195(4275):302–4.
- [52] Tryoen-Toth P et al. Viability, adhesion, and bone phenotype of osteoblast-like cells on polyelectrolyte multilayer films. *J Biomed Mater Res* 2002;60:657–67.
- [53] Murray N, Dunand D. Effect of thermal history on the superplastic expansion of argon-filled pores in titanium: Part I Kinetics and microstructure. *Acta Mater* 2004;52(8):2269–78.
- [54] Murray NGD, Dunand DC. Effect of thermal history on the superplastic expansion of argon-filled pores in titanium: Part II Modeling of kinetics. *Acta Mater* 2004;52(8):2279–91.
- [55] Li H, Oppenheimer S, Stupp SI, Dunand DC, Brinson LC. Effects of pore morphology and bone ingrowth on mechanical properties of microporous titanium as an orthopedic implant material. *Mater Trans* 2004;45(4):1124–31.
- [56] Li JP, Li SH, de Groot K, Layrolle P. Preparation and characterization of porous titanium. *Bioceramics* 2002;14:51–4.
- [57] Wen C, Yamada Y, Shimojima K, Chino Y, Hosokawa H, Mabuchi M. Novel titanium foam for bone tissue engineering. *J Mater Res* 2002;17(10):2633–9.
- [58] Pavlin D, Dove SB, Zadro R, Gluhak-Heinrich J. Mechanical loading stimulates differentiation of periodontal osteoblasts in a mouse osteoinduction model: effect on type I collagen and alkaline phosphatase genes. *Calcif Tissue Int* 2000;67(2):163–72.
- [59] Weyts FAA, Bosmans B, Niesing R, van Leeuwen J, Weinans H. Mechanical control of human osteoblast apoptosis and proliferation in relation to differentiation. *Calcif Tissue Int* 2003;72(4): 505–12.
- [60] Wolf S, Augat P, Eckert-Hubner K, Laule A, Krischak GD, Claes LE. Effects of high-frequency, low-magnitude mechanical stimulus on bone healing. *Clin Orthop Relat Res* 2001;385:192–8.